Surfactant Control of Interfacial Reaction Rates in Aqueous Microdroplets

Alexander M. Prophet,[1] David T. Limmer,[1,2,3,4] & Kevin R. Wilson[1*]

[1]*Chemical Sciences Division, Lawrence Berkeley National Laboratory, Berkeley, CA 94720*

[2]*Department of Chemistry, University of California, Berkeley, CA 94720*

[3]*Materials Science Division, Lawrence Berkeley National Laboratory, Berkeley, California 94720*

[4]*Kavli Energy NanoScience Institute, Berkeley, California 94720*

Abstract

Microdroplets are purported to enhance reaction rates and produce spontaneous chemical transformations that are unfavorable in macroscale systems. The gas-liquid interface is widely implicated for the emergence of these chemical anomalies. Experiments conducted on individual microdroplets provide a unique platform for studying interfacial effects while bypassing transport limitations often encountered in macroscopic systems. We investigate such interfacial effects by analyzing the suppression of the I^- + O_3 surface reaction by the nonionic surfactant Triton X-100 in an array of levitated microdroplets. Using a novel kinetic framework describing surface and bulk reactivity, we find that increasing surfactant concentration shifts the locus of reaction from the top-most nanometer of the interface to a subsurface region located < 2 nm below the surface. This detailed picture of spatial reactivity is afforded only by considering the timescales for O_3 adsorption and solvation combined with reaction monitoring in single microdroplets. Chemical uniqueness is further illustrated by the I^- + O_3 rate dependence on [Triton X-100], which is quantitatively understood by considering finite size effects in microdroplets. Both size and surface effects are considered to derive an analytical expression for reactive uptake of O_3 which demonstrates the role of competitive adsorption of Triton-X and I^- at the gas-liquid interface. This work establishes a novel approach to understanding interfacial reaction kinetics that successfully links nanometer-scale dynamics from molecular simulations with macroscale measurements of surface tension and microscale measurements of chemical reactivity.

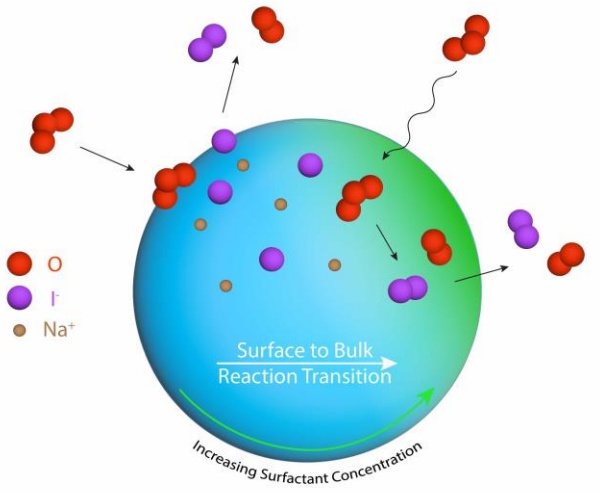

I. Introduction

Microdroplets present unique chemical environments and are reported to exhibit unexpectedly rapid reaction kinetics.[1–3] These kinetics are generally difficult to interpret in many experiments as reactive contributions from the gas, bulk liquid, and interface are not easily distinguished, which has been shown to lead to erroneous conclusions about microdroplet reactivity.[4–6] Key kinetic parameters such as reagent concentrations, droplet radii, and the rates of gas-liquid partitioning and evaporation are also difficult to constrain in spray-type microdroplet experiments—leading similarly to exaggerated claims of interfacial reactivity.[7,8] Furthermore, there is an ongoing debate around the evidence for and mechanism of "spontaneous" chemistry that is attributed to strong electric fields.[9–14]

Reaction rates at the gas-liquid interface do, however, likely deviate from their bulk analogs. Reagent concentrations at the interface are known to differ from those in the bulk solution for many molecules due to their unique thermodynamic stability at the interface[15–19] or from the kinetics of competing diffusion and adsorption timescales.[20–22] Surfactant molecules exhibit an extreme preference for the gas-liquid interface due to their chemical structure, the consequences of which are important for understanding the dynamic surface tension of microdroplets and the activation of cloud condensation nuclei.[23–29] Surface tension measurements on surfactant-containing microdroplets have revealed unique static properties originating from finite-volume effects in pico-liter volumes.[30–32] Additionally, recent work by Bain et al.[33] interrogating the dynamics of surfactant adsorption has shown that timescales for interfacial equilibration span up to milliseconds for freshy generated microdroplets with radius $r \sim 25$ μm.

Interfacial reaction rates may also be strongly influenced by dynamics at the interface. For multiphase reactions, molecular motions on the top-nanometer of solution can significantly alter a reaction trajectory compared to a purely bulk-dominated process.[34,35] Furthermore, the energetics of the reaction coordinate itself may be influenced by the partially solvated environment of the interface,[36,37] although empirical validation of this effect is limited. Our previous investigations of iodide oxidation kinetics in microdroplets[38,39] indeed suggest that partial-solvation of the $I^- + O_3$ reaction at the interface yields a reaction efficiency resembling the gas-phase,[40] rather than the aqueous-phase. Nevertheless, direct probes of interfacial chemistry are necessary to verify such observations and provide a basis for identifying general trends needed to link reaction efficiency to the degree of solvation. Given the number of uncertainties surrounding surface reactivity, there remains a need for novel kinetic methods and detailed models of chemistry at microdroplet interfaces.[41]

Here we report on the coupling of a prototypical surface reaction (I^- + O_3) with interfacial adsorption of the nonionic surfactant Triton X-100 (TX) in microdroplets. Kinetic measurements demonstrate that the reaction is effectively inhibited by addition of [Triton X-100], with reactivity switching from the surface to the subsurface. This system is chosen since the ozonation of iodide in aqueous solution is a relatively well characterized system[42–44] that exhibits chemical reactivity at the interface under acidic conditions.[39] Similarly, Triton X-100 is a common surfactant whose interfacial properties in both bulk aqueous systems and in microdroplets is well characterized.[30,45–47] The inhibition of the surface reaction with increasing [TX] results from the competition of TX with I^- at the gas-liquid interface, which is accompanied by "bulk depletion" of surfactant throughout the microdroplet volume.[30,31]

To quantitatively explain the experimental observations, a multiphase reaction model is used to replicate the microdroplet kinetics using explicit simulations. This multiphase model is also used to derive analytical expressions for predicting reactive uptake. The coupled chemical and mass-transport framework used in this model is adapted from previous work on the I^- + O_3 reaction in droplets for varying reagent concentrations and pH.[38,39] This framework also includes the spatial partitioning of the gas-phase, aqueous surface, subsurface region, and bulk interior in order to isolate the reactive contributions of each. Fig. 1A conceptually outlines the workings of the model, where O_3 adsorption and desorption at the interface couple to the surface reaction, solvation, and the subsurface reaction. This conceptual framework is used to predict the chemical kinetics using stochastic reaction-diffusion simulations (as has been explored extensively with this particular reaction system)[38,39] and to derive an analytical expression for reactive uptake that includes interfacial effects of Triton X-100. Molecular properties at the interface are parameterized in the model using average density profiles from molecular dynamics simulations (MD), as illustrated in Fig. 1B, and by macroscale surface tension measurements of Triton X-100. Consequently, the reaction location can be identified with high fidelity, as summarized in Fig. 1, where the overall uptake of O_3 is controlled by the surface reaction for low [TX] and by liquid diffusion of O_3 into the sub-surface region at high [TX] (extending < 2 nm beneath the surface).

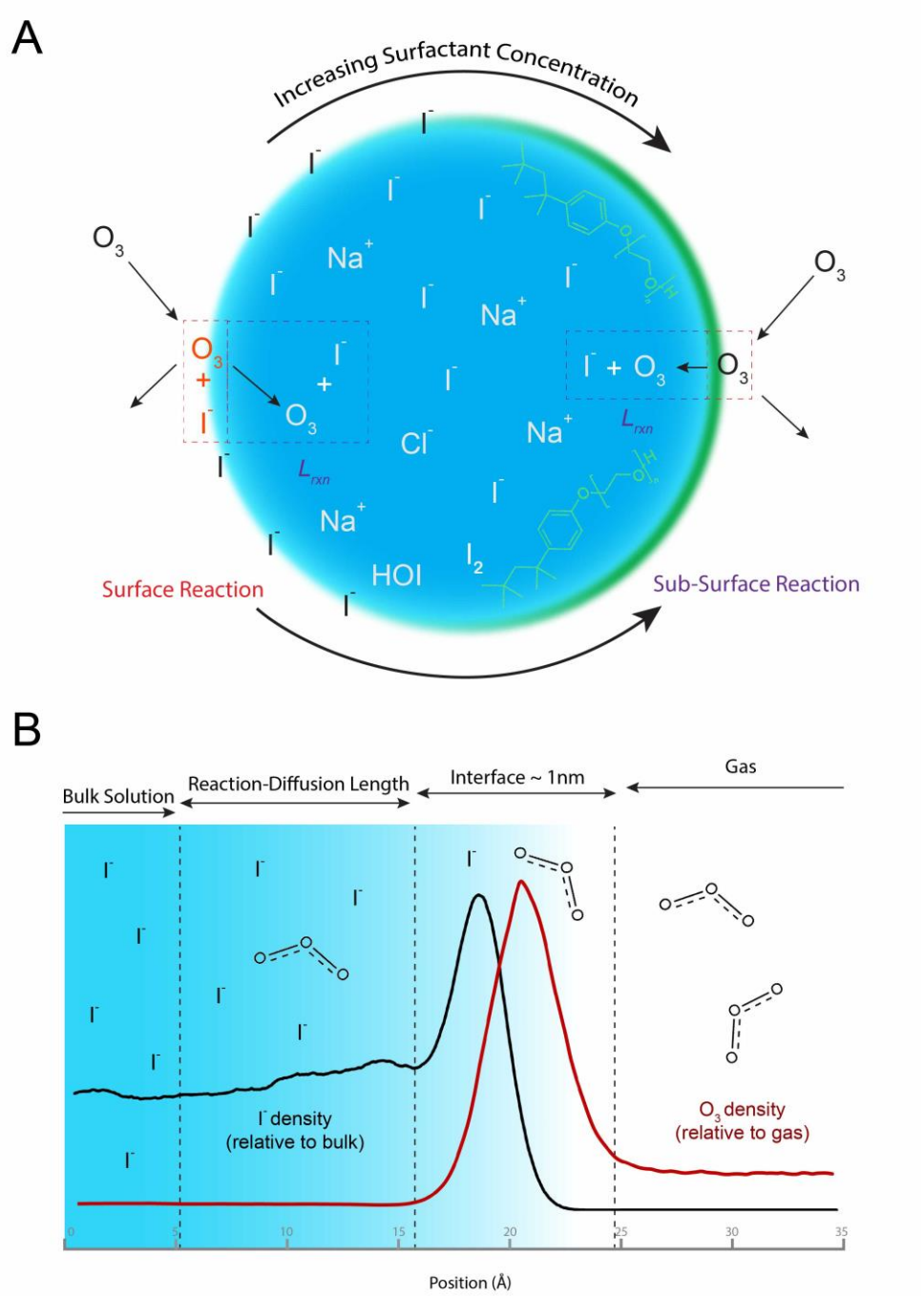

Fig. 1: (A) Model droplet undergoing oxidation with increasing surfactant concentration. Higher concentrations of surfactant inhibit the surface reaction and reactivity in the subsurface region dominates. (B) Conceptual scheme of the droplet interface showing I^- density extending into the bulk solution, and O_3 density in the gas phase from Prophet et al.[39] Density profiles for these reagents are normalized with respect to their bulk phase densities, and both show some degree of density enhancement at the interface. Notably, the density profiles overlap across the ~ 1 nm range where the overall density attenuates, which we identify herein as the surface. The subsurface region we denote as the "reaction-diffusion" region as this extends the length of the reaction-diffusion length as defined for O_3 under the experimental salt concentration, of L_{RD} = 1.36 nm.

II. Experimental

Microdroplet oxidation kinetics are measured in a quadrupole electrodynamic trap (QET)[48] equipped with an open-port sampling interface (OPSI) for single droplet mass spectrometry (MS).[38] This particular assembly is recently described in multiple works, along with comparable configurations.[38,49,50] The QET charges and traps individual microdroplets generated from a piezo-electric droplet dispenser (Microfab). Arrays of ~100 microdroplets are trapped while a gas phase oxidant is introduced to the enclosed assembly, initiating the reaction. Single microdroplets are then sized via Mie scattering[51,52] before being ejected from the QET into the OPSI-MS. Droplet signals obtained from OPSI-MS allow for the quantitative determination of the solute consumed during the reaction. Additional information and a schematic of the experimental apparatus is provided in supplemental information section SI-1.

The ion signal from iodide (m/z = 126.89) is shown in Fig. 2A, with example mass spectra before and after the reaction in SI-1. Peak areas, integrated from the time-series, are used to quantify the [I^-] in individual droplets during exposure to O_3, as shown in Fig. 2B. Microdroplets are prepared from solutions that contain NaI and citric acid to buffer the pH at 3. NaCl is added to the solution to maintain constant water activity and therefore droplet size over the course of reaction. For these experiments, the humidity of the trap was maintained at 88%, and hence, the final water activity in the microdroplets is a_w = 0.88. Using this final water activity and the radius of the droplet, the initial droplet concentrations are: $[NaI]_0$ = 795 mM, 1 M NaCl, and 1M citric acid/sodium citrate. Triton X-100 is added to the initial droplet solution in a concentration range of 6 μM to 1.6 mM. Stock solutions containing surfactant were first prepared via serial dilution, before adding salt solution to obtain the final concentration.

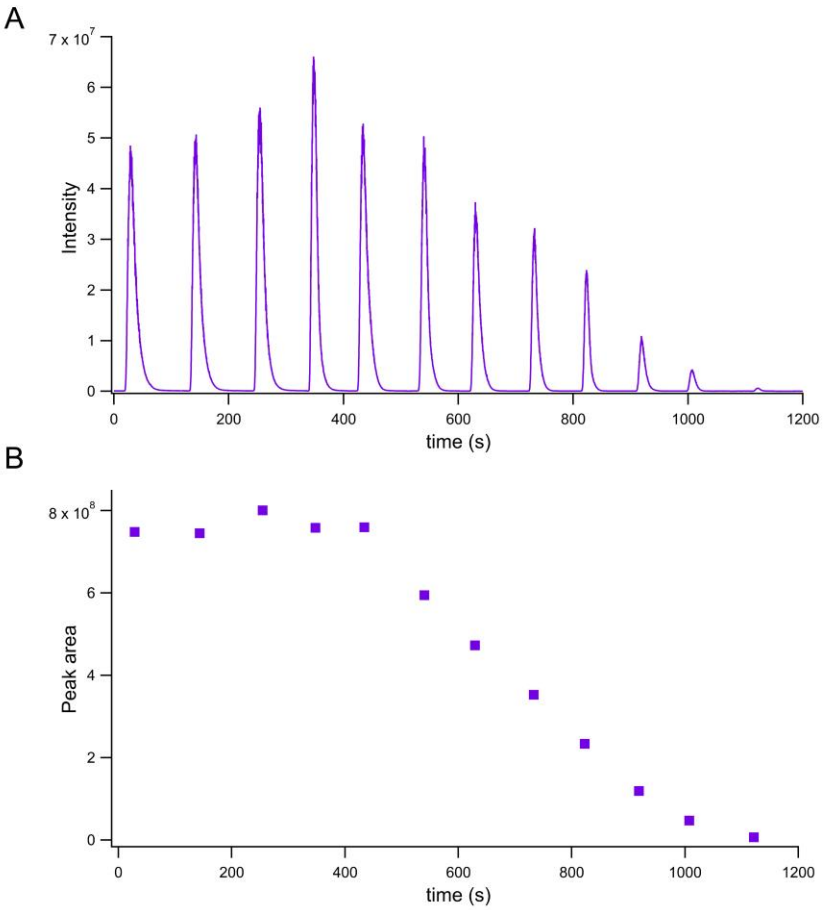

Fig. 2: Microdroplet detection events using OPSI-MS. Panel A shows a droplet detection time-series where initial, unreacted droplets are first detected, followed by iodide decay resulting from O_3 exposure. Panel B shows peak areas from overall intensity trace in A.

III. Results

Iodide consumption kinetics as a function of [TX] are shown in Fig. 3. Fig. 3A shows that the reaction slows when increasing [TX] from 32 μM to1.6 mM. The entire experimental dataset across a broad range of [TX] (6 μM to 3.2 mM) is shown in Fig. 3B. The O_3 concentration for all experiments is 500 ± 10 ppb and initial droplet radii are r = 17 ± 1 μm. As shown in Fig. 3, the overall rate of I^- decay decreases with increasing [TX]. For comparison, explicit kinetic simulations are included for each reaction condition in Fig. 3. These simulations use a previously validated kinetic model for iodide oxidation in microdroplets,[39] augmented with an additional step to include Triton X-100 adsorption to the air-water interface. Details of the kinetic model and an overview of the Triton X-100 adsorption description are included in the following analysis section.

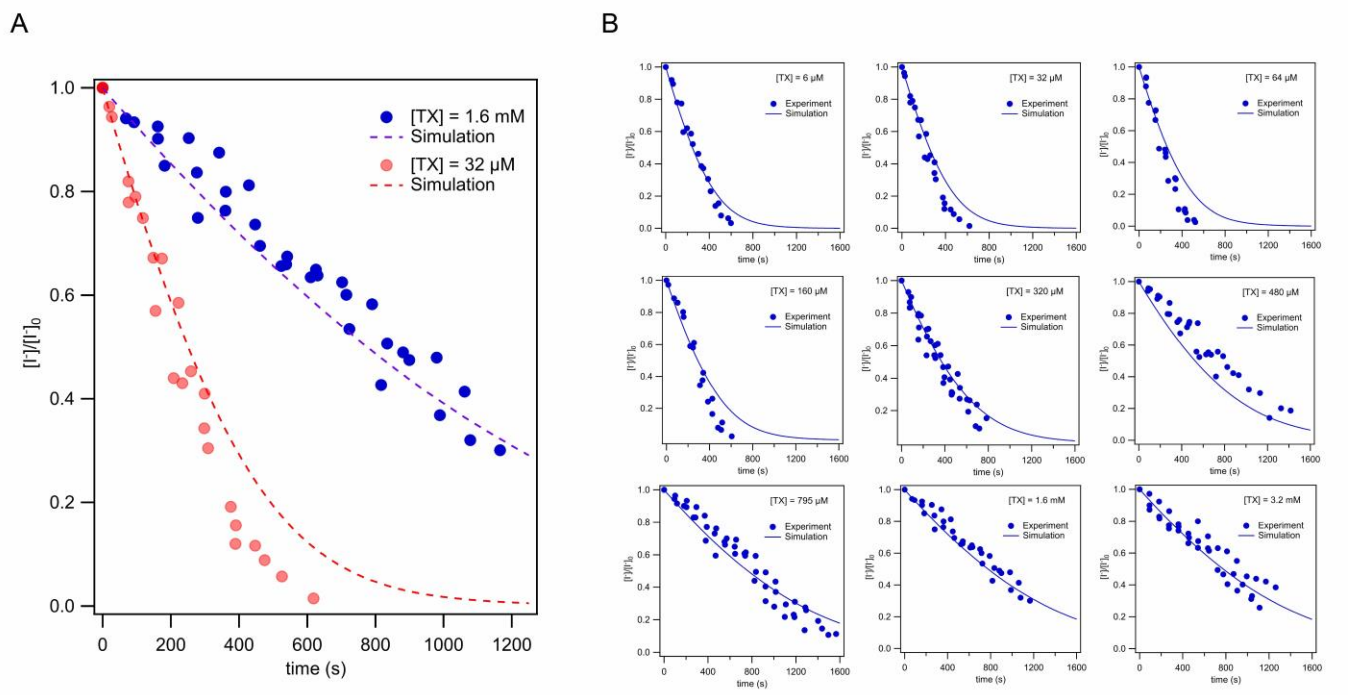

Fig. 3: Experimental decay profiles of $[I^-]$ in microdroplets during O_3 oxidation. Panel (A) shows side-by-side results for a high and low [TX] condition. Panel (B) provides individual kinetics for each condition. Experimental data is shown as points and simulation output as lines. All experiments are on 17 µm radius aqueous droplets containing 795 mM [NaI] and variable Triton-X concentrations when exposed to 500 ppb $[O_3]$.

The initial rate of decay, k_{init}, of iodide in each experiment is used to compute reactive uptake coefficients γ_{exp} for O_3,[53]

$$\gamma_{exp} = \frac{4 \cdot r \cdot k_{init} \cdot \left[I^-_{(b)}\right]_0}{3 \cdot [O_{3(g)}] \cdot \bar{c}} \qquad \text{Eq. 1}$$

where r is the droplet radius and $\bar{c}$ the mean speed of O_3 in the gas-phase. Uptake coefficients are shown in Fig. 4 and exhibit a non-linear dependence on [TX]. For [TX] < 100 µM, the reaction kinetics are largely insensitive to the addition of TX with the observed uptake of $\gamma_{exp} \sim 5.5\times10^{-3}$, a value that is equivalent for the same sized microdroplets in the absence of [TX].[39] For 100 µM < [TX] < 500 µM, there is a sharp transition with the observed uptake decreasing to $\sim1.5\times10^{-3}$. Increasing the [TX] beyond 500 µM has no noticeable effect on the uptake coefficient. This behavior is consistent with the simple picture that increasing TX displaces iodide from the surface, which effectively shuts off the surface reaction for [TX] ≥ 500 µM. The plateau observed for higher [TX] indicates that once the surface is saturated with TX, only reactivity within the sub-surface of the microdroplet contributes to the net loss of I^-, thus yielding

a smaller uptake coefficient. Although one might predict that this saturation point should coincide with the CMC of Triton X-100 in bulk solution (~200 μM), this shift in the observed saturation behavior to larger [TX] (~500 μM) is a consequence of surfactant adsorption in finite-sized droplets, which is discussed in the following section.

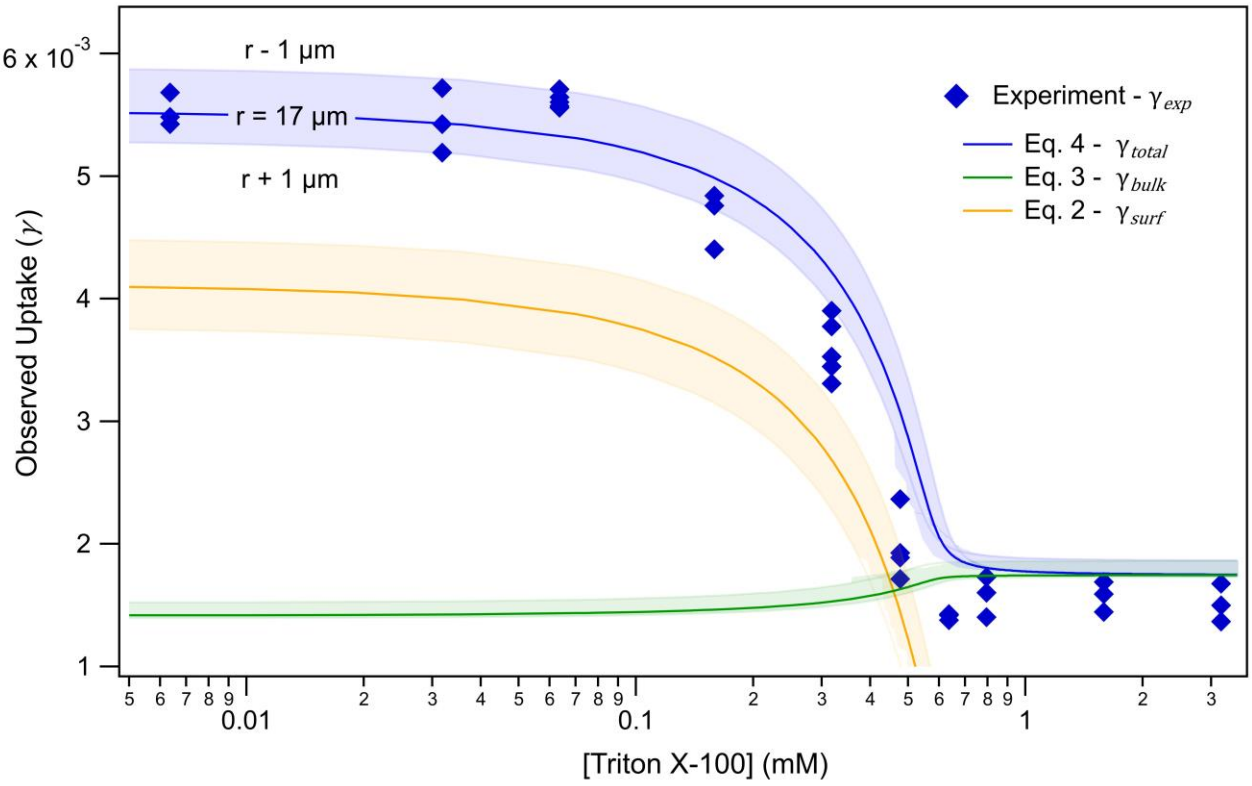

Fig. 4: Experimental kinetics summarized using reactive uptake coefficients of O_3 for the range of droplet [Triton X-100] studied. Analytical expressions Eq. 2-4 are compared to experimental values. Error bars indicated around model results represent the predicted values for ± 1 μm in radius.

IV. Analysis

The experimental results shown in Fig. 3 and summarized in Fig. 4 qualitatively suggest that the addition of TX inhibits the $I^- + O_3$ reaction at the air-water interface. To understand this more quantitatively, a competitive adsorption model of I^- and TX is developed. This model utilizes the same multiphase kinetic framework used to execute the explicit kinetic simulations in Fig. 3. The kinetic simulations are performed using Kinetiscope (https://hinsberg.net/kinetiscope/), as discussed extensively in previous publications.[38,39,49] The specific reaction mechanism used here and the spatial representation of a droplet within Kinetiscope can be found in Prophet *et al.*[39] The mechanism consists of the primary oxidation of the iodide anion by O_3 followed by a series of secondary chemical steps that ultimately

produce I_2 at pH 3. Chemically relevant kinetic regions of the microdroplet are identified, including the surface, sub-surface, and inner bulk, with mass-transport kinetics defined at the interface and between each adjacent region. The dimensions of the interfacial region is approximated using the density attenuation across the interface as observed in MD.[39] The sub-surface length is defined using the reaction-diffusion length of O_3 in solution. The reaction-diffusion length, as previously discussed,[54–56] is the average distance an O_3 molecule diffuses in solution prior to undergoing a reaction. Kinetic steps describing mass transport of the reactants and solutes at the interface are also described, constrained by MD and previously reported values. Here, kinetic steps are added to model Triton X-100 adsorption to the interface. Since the kinetic model and simulation methods have been thoroughly described in recent work, we instead emphasize the introduction of analytical expressions for uptake coefficients at the surface and within the reaction-diffusion region below. These uptake expressions rely on previous work and are augmented here with the addition of steps to describe TX adsorption.[57]

Formulation of Uptake Coefficients

Reactive uptake coefficients γ_s and γ_{rd} resulting from O_3 loss at the droplet surface (s) and within the reaction-diffusion length (L_{rd}), are adapted from expressions found in Wilson et al.,[57]

$$\gamma_s = \frac{4 \cdot r \cdot k_{rxn}^{srf} \cdot \left[O_{3(ads)}\right]\left[I^-_{(ads)}\right]}{3 \cdot \bar{c} \cdot \left[O_{3(g)}\right]} \cdot \frac{r^3 - (r-\delta)^3}{r^3} \quad \text{Eq. 2}$$

$$\gamma_{rd} = \frac{4 \cdot r \cdot k_{rxn}^{blk} \cdot \left[O_{3(rd)}\right]\left[I^-_{(rd)}\right]}{3 \cdot \bar{c} \cdot \left[O_{3(g)}\right]} \cdot \frac{(r-\delta)^3 - (r-\delta-L_{rd})^3}{r^3} \quad \text{Eq. 3}$$

$$\gamma_{total} = \gamma_s + \gamma_{rd} \quad \text{Eq. 4}$$

where δ is the surface thickness of 1 nm and L_{rd} is the reaction-diffusion length of O_3 in solution under our experimental conditions, *i.e.*, $L_{rd} = \sqrt{\frac{D}{k_{rxn}^{blk} \cdot [I^-]_0}} = 1.36$ nm. Equations 2 and 3 adopt the same general form in which a reaction term is defined using local concentrations (indicated with subscripts *s* or *rd* to denote the relevant region), normalized by the O_3 collisional flux on the droplet surface. Each equation has a volumetric weighting term to account for the relative fraction of the entire droplet volume that is kinetically active (i.e., surface or reaction-diffusion region). We note that there is an additional contribution, γ_b, to the overall uptake arising from the inner bulk (b) or "core" of the droplet, beyond the depth of the reaction diffusion length L_{rd} (the core, in fact, comprises the vast majority of the droplet

volume). Since L_{rd} has nanometer dimensions for the current experiments, virtually all of the reactivity occurs either at the surface or within the reactive diffusive (RD) volume. Therefore, we can neglect the uptake contribution of γ_b in the following analysis. Fig. 5 provides a geometric overview of the droplet regions, with length scales and the corresponding γ for each region.

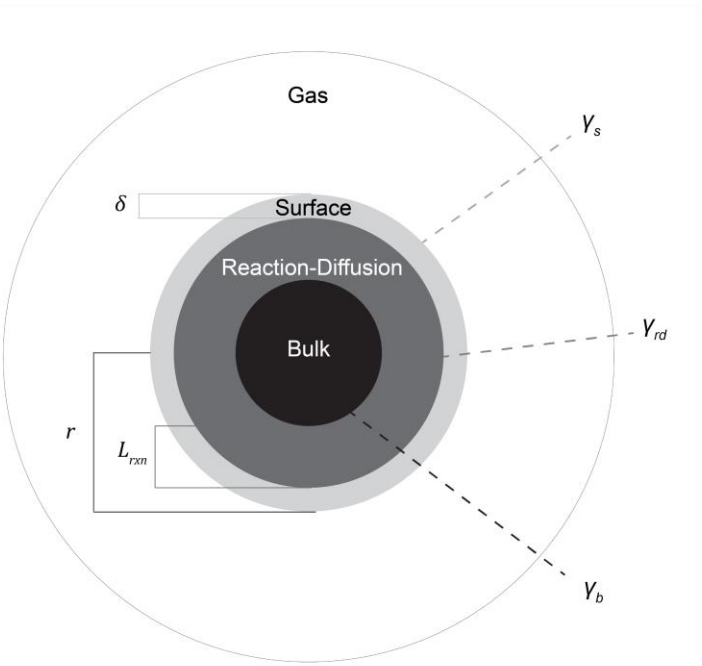

Fig. 5: Conceptual overview of microdroplet spatial regions (not to scale), with respective defining lengths and uptake coefficients labeled. As noted above, the uptake contribution from the inner core is neglected in the present work due to the much larger values of γ_s and γ_{rd}.

Application of Eqs. 2 and 3 requires calculating [$I^-_{(ads)}$] and [$O_{3(ads)}$] in the surface region, and [$I^-_{(rd)}$] and [$O_{3(rd)}$] in the RD region. This is done by applying a steady-state assumption to the kinetic framework used in the stochastic simulations, as described in detail in section SI-3. We assume that shortly after the reaction has begun, local concentrations of reactants in each geometric region rapidly achieve steady-state. These steady-state concentrations are governed by the balance of mass transport (source) and chemical reactivity (sink). The governing transport kinetics rely heavily on both gas- and liquid-phase diffusion of O_3, as well as the desorption and solvation kinetics across the energetic barrier at the interface. For the solutes I^- and TX, diffusional transport is simpler, and the droplet can be assumed to be well-mixed since the transport rate of I^- from the bulk to the surface is larger than the surface-loss rate under our experimental conditions. This is generally a reasonable approximation when the aqueous reactant concentration (*i.e.,* iodide) is many orders of magnitude larger than that of the solubilized trace gas. In this

case, the steady-state subsurface concentration in the RD region, $[I^-_{(rd)}]$, is simply the initial bulk concentration $[I^-_b]_0$.

Assuming the interfacial concentration of I^- is not perturbed by the reaction (also generally true when a trace gas reacts with a concentrated solute), the steady-state surface-adsorbed concentration of iodide $[I^-_{(ads)}]$ can be described by a Langmuir competitive-adsorption isotherm,[58]

$$\left[\mathrm{I}^-_{(ads)}\right] = \frac{\Gamma_\infty^{\mathrm{I}^-}}{\delta} \cdot \frac{K_{eq}^{\mathrm{I}^-} \cdot \left[\mathrm{I}^-_{(bulk)}\right]}{1 + K_{eq}^{\mathrm{I}^-} \cdot \left[\mathrm{I}^-_{(bulk)}\right] + K_{eq}^{TX} \cdot \left[\mathrm{TX}_{(bulk)}\right]} \qquad \text{Eq. 5}$$

where $\Gamma_\infty^{\mathrm{I}^-}$ represents the maximum coverage term (in molecules/cm^2) of iodide at the interface, expressed as a volumetric concentration by dividing by the surface thickness δ. $K_{eq}^{\mathrm{I}^-}$ is the Langmuir adsorption equilibrium constant, which relates the bulk concentration of I^- to the surface adsorbed concentration. Similarly, K_{eq}^{TX} is the equilibrium constant relating the bulk and surface concentrations of TX and the quantity Γ_∞^{TX} the corresponding maximum coverage term. Values of $K_{eq}^{\mathrm{I}^-}$ and $\Gamma_\infty^{\mathrm{I}^-}$ are taken from recent work,[39] where MD simulations were used to quantify interface densities of I^- as a function of bulk concentration.

Triton X-100 Adsorption Description

To constrain the adsorption behavior of TX in the model, Γ_∞^{TX} and K_{eq}^{TX} are obtained from fits of surface tension measurements of aqueous TX solutions[30] using the Szyszkowski equation-of-state (EOS),[59]

$$\gamma - \gamma_{0.5\mathrm{M\ NaCl}} = -\Gamma_\infty^{TX} \cdot R \cdot T \cdot \ln(1 - \theta) \qquad \text{Eq. 6}$$

where R is the gas constant, T the temperature, and $\gamma_{0.5\mathrm{M\ NaCl}}$ is the surface tension of 0.5 M NaCl solution. This EOS depends on a fractional surface coverage (θ). Here, we model θ with a standard Langmuir adsorption isotherm:

$$\theta = \frac{K_{eq}^{TX} \cdot \left[TX_{(bulk)}\right]}{1 + K_{eq}^{TX} \cdot \left[TX_{(bulk)}\right]}. \qquad \text{Eq. 7}$$

Fig. 6 shows surface tension measurements of a 0.5 M NaCl solution as a function of [TX] measured by Bzdek et al.[30] Also shown are fits to Eq. 6, which yield $\Gamma_\infty^{TX} = 2\times10^{14}$ molecules/cm^2 and

K_{eq}^{TX} = 1.1×10^{-15} cm^3 molecule^{-1} s^{-1}. The kinetic model is adapted to include this information by defining a surface partitioning step for Triton X-100,

$$\mathrm{TX}_{(bulk)} + \mathrm{site} \underset{k_{solv}}{\overset{k_{desolv}}{\rightleftarrows}} \mathrm{TX}_{(ads)}. \qquad (S1)$$

Site in step (S1) is defined as previously discussed for O_3 and I^-,[38,49,57] where the maximum surface coverage Γ_∞^{TX} constrains the site area and related volumetric concentration within the model geometry. Kinetic coefficients k_{desolv} and k_{solv} are directly related to the Langmuir adsorption equilibrium coefficient: $K_{eq}^{TX} = k_{desolv}/k_{solv}$. While the equilibrium coefficient only constrains the ratio, we choose a value of k_{solv} = 1 s^{-1} to constrain k_{desolv}. This choice of k_{solv} falls within the range of timescales from previous measurements,[33,60] although we note there exists substantial deviation in these timescales for different surfactants, and a unique measurement for Triton X-100 has not been made to the best of our knowledge. Fortunately, the model results are insensitive to the absolute values of k_{solv} and k_{desolv} since the experimental time-scale is much longer than the equilibration time of the surfactant at the interface, which is expected to be on the order of milliseconds.[33]

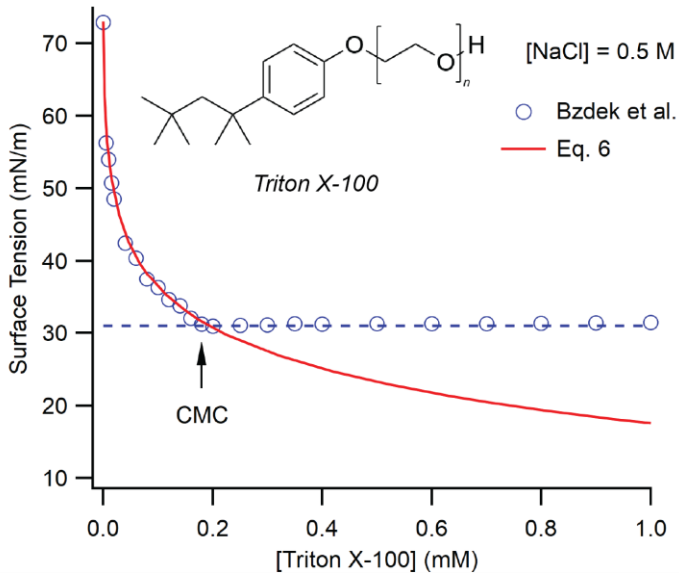

Fig. 6: Surface tension measurements by Bzdek et al. of Triton X-100 solution in 0.5 M NaCl above and below the CMC ~ 0.2 mM. A fit to Eq. 6 is obtained to provide the maximum surface coverage Γ_∞^{TX} and Langmuir adsorption equilibrium coefficient K_{eq}^{TX} that are used directly in the kinetic model. The molecular structure of Triton X-100 is provided, where *n* has an average value of 9.5.

Surface Adsorption Coupling to Bulk Depletion in Microdroplets

Benchmarked to macroscopic measurements, the partitioning of TX to the interface can be modeled in microdroplets using the same general mechanism. An important consequence of applying this description to microscale volumes is that the surface coverage diverges from that expected for macroscale solutions.[56] This is because microdroplets lack the total number of TX molecules required to satisfy the equilibrium surface coverage observed in a macroscale solutions. This is shown in Fig. 7A, where divergence from the macroscopic behavior becomes quite pronounced in small droplets. This finite-volume effect arises from the depletion of surfactant concentration in the bulk interior as the surfactant partitions to the droplet interface.[61] Considering surface-to-volume constraints for a single droplet radius and the partitioning kinetics parametrized above for TX, a simple expression for adsorbed concentration[56] and the corresponding depleted bulk concentration is (see section SI-3 for derivation),

$$[\mathrm{TX}]_{(ads)} = \frac{1}{2 \cdot N_1} \cdot \left(N_2 - \sqrt{N_2^2 - 4 \cdot N_1 \cdot N_3} \right) \qquad \text{Eq. 8}$$

$$[\mathrm{TX}]_{(bulk)} = [\mathrm{TX}]_0 - \left(\frac{3\,\delta}{r} \right) \cdot \frac{1}{2 \cdot N_1} \cdot \left(N_2 - \sqrt{N_2^2 - 4 \cdot N_1 \cdot N_3} \right) \qquad \text{Eq. 9}$$

where,

$$N_1 = 3 \cdot k_{desolv} \cdot \delta^2 \qquad \text{Eq. 10a}$$

$$N_2 = 3 \cdot k_{desolv} \cdot \Gamma_\infty^{TX} \cdot \delta + k_{desolv} \cdot [\mathrm{TX}]_0 \cdot \delta \cdot r + k_{solv} \cdot \delta \cdot r \qquad \text{Eq. 10b}$$

$$N_3 = k_{desolv} \cdot \Gamma_\infty^{TX} \cdot [\mathrm{TX}]_0 \cdot r \qquad \text{Eq. 10c}$$

In Eqs. 8-10c, $[\mathrm{TX}]_0$ is the nominal concentration of Triton X-100, equivalent to the bulk concentration in the absence of finite-volume effects. This nominal concentration $[\mathrm{TX}]_0$ is taken as the independent quantity and is plotted as the domain in Figs. 7A and B. Eq. 8 provides the equilibrium surfactant concentration at the interface, whereas Eq. 9 provides an expression for the corresponding equilibrium bulk concentration in the droplet. This demonstrates how the true bulk concentration $[\mathrm{TX}_{(bulk)}]$ in the microdroplet deviates from the nominal bulk concentration $[\mathrm{TX}]_0$ as the droplet radius decreases, shown for an array of sizes and concentrations in Fig. 7B. This equilibrated concentration $[\mathrm{TX}_{(bulk)}]$ computed by

Eq. 9 is the relevant bulk concentration to describe competitive adsorption between I^- and TX. As such, the expression for $[TX_{(bulk)}]$ is used in Eq. 5 to accurately model the adsorbed concentration of I^- as a function of both $[I^-_{(bulk)}]$ and $[TX_{(bulk)}]$ in the droplet.

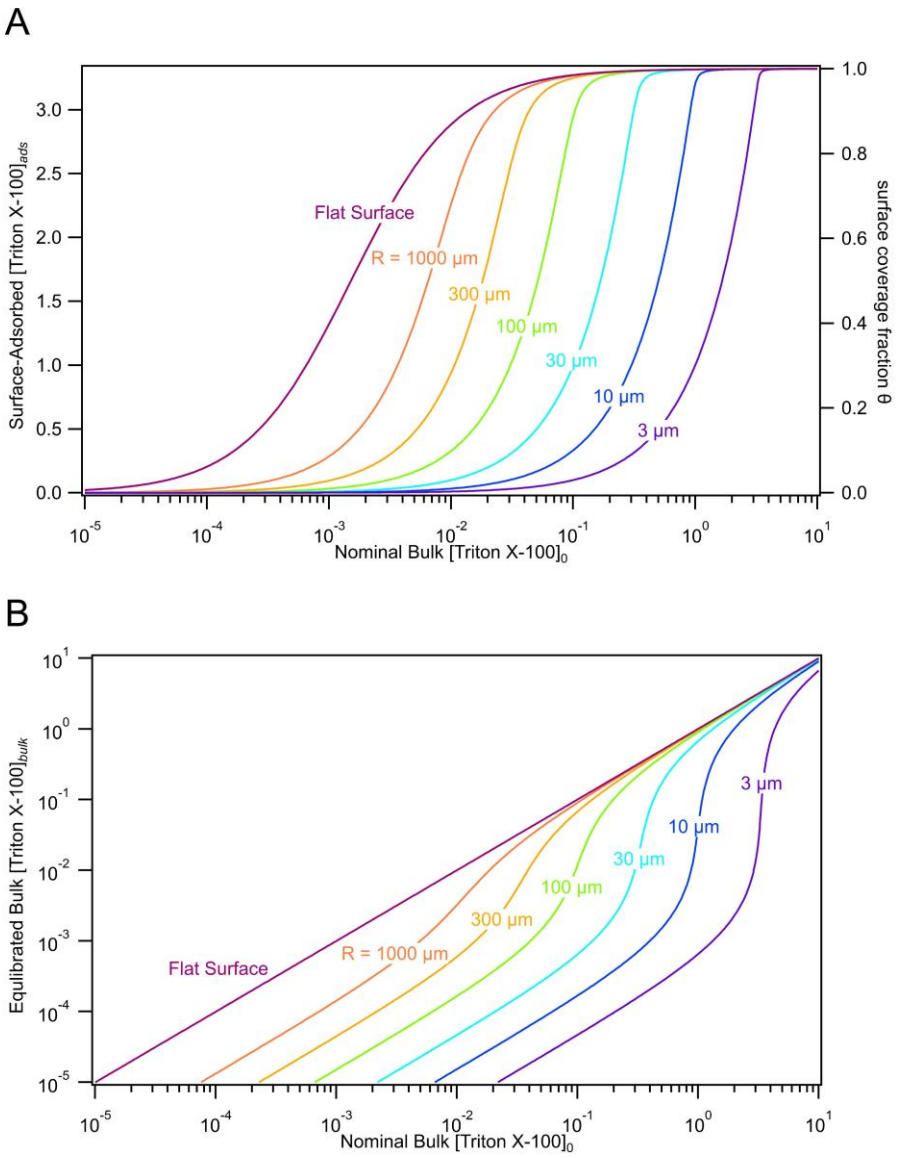

Fig. 7: Panel (A) shows the surface-adsorbed concentration (or fractional surface coverage) for [Triton X-100] ranging from 10^{-5}-10 mM in droplets with various radii. The suppression of coverage fraction for smaller microdroplets is a finite-volume effect, where adsorption to the interface is coupled to depletion of the bulk concentration. This is also demonstrated in panel (B), where the equilibrium [TX] is shown vs the nominal bulk concentration. For both of these panels, the nominal bulk $[\text{Triton X-100}]_0$ axis indicates the bulk concentration of the droplet in the absence of any surface adsorption. Importantly, the true bulk concentration at equilibrium can be greatly depleted relative to the nominal concentration, as demonstrated in (B).

Using $[I^-_{(ads)}]$ (Eq. 5) and $[I^-_{(rd)}]$ (simply the bulk iodide concentration $[I^-_{(bulk)}]_0$), the steady-state concentrations of O_3 in the respective regions can be computed. This is accomplished by applying a quasi-steady-state condition to the entire kinetic framework as detailed in SI-3. Resulting concentrations are defined in terms of the rate coefficients for the surface- and bulk-reaction (k_{rxn}^{surf}, k_{rxn}^{bulk}) and coefficients that describe gas-diffusion (k_{diff}^{gas}), liquid-diffusion (k_{diff1}^{liq}, k_{diff2}^{liq}), adsorption and desorption from the gas to the interface (k_{ads}, k_{des}), and desolvation/solvation from the liquid to the interface (k_{desolv}, k_{solv}).

$$[O_{3(ads)}] = \frac{\left(\frac{k_{diff}^{gas}\, k_{ads}}{k_{diff}^{gas} + k_{ads}}\right)[O_{3(g)}]}{k_{des} + k_{solv} + [I^-_{(ads)}]k_{rxn}^{surf} - \left(\frac{k_{des}\, k_{ads}}{k_{diff}^{gas} + k_{ads}}\right) - \left(\frac{k_{desolv}\, k_{solv}}{k_{diff1}^{liq} + k_{desolv}}\right) - \left(\frac{k_{diff1}^{liq}\, k_{diff2}^{liq}\, k_{desolv}\, k_{solv}}{\left(k_{diff2}^{liq} + k_{desolv}\right) \times \left(k_{desolv}\,[I^-_{(rd)}]\, k_{rxn}^{bulk} + k_{diff1}^{liq}[I^-_{(rd)}]k_{rxn}^{bulk} + k_{diff2}^{liq}\, k_{desolv}\right)}\right)}$$

Eq. 11

$$[O_{3(rd)}] = \frac{k_{diff2}^{liq}\, k_{solv}\, [O_{3(ads)}]}{k_{desolv}\, [I^-_{(rd)}]\, k_{rxn}^{bulk} + k_{desolv}\, k_{diff2}^{liq} + k_{diff1}^{liq}[I^-_{(rd)}]\, k_{rxn}^{bulk}} \quad \text{Eq. 12}$$

Note that Eq. 12 is defined implicitly in terms of the adsorbed ozone concentration in Eq. 11 for the sake of brevity.

The rate coefficients in Eq. 11 and Eq. 12 are explained in more detail in Prophet *et al.*[39] and in supplemental section SI-3. Briefly, the reaction rate $k_{rxn}^{bulk} = 1.2\times10^9$ M^{-1} s^{-1} is from previous literature [43,44] and $k_{rxn}^{surf} = 6\times10^7$ M^{-1} s^{-1} is obtained from our previous work, which found evidence for diminished surface reactivity.[39] The pairs of kinetic constants k_{solv}/k_{desolv} and k_{des}/k_{ads} are obtained by an analysis of the timescales associated with molecular motions in MD simulations of O_3 at the air-water interface.[38,62] The gas-diffusion rate k_{diff}^{gas} is calculated by considering the flux of O_3 to the droplet surface, as discussed in Prophet *et al.*,[39,63] and liquid-diffusion rates k_{diff1}^{liq}, and k_{diff2}^{liq} are computed using Fick's first law.[64] These terms are expressions involving the diffusion constants over relevant length scales,

$$k_{diff}^{gas} = \frac{D_{gas}}{r\,\delta}, \quad \text{Eq. 13}$$

$$k_{diff1}^{liq} = \frac{2\,D_{liq}}{(L_{RD}+\delta)\delta}, \quad \text{Eq. 14}$$

$$k_{diff2}^{liq} = \frac{2\,D_{liq}}{(L_{RD}+\delta)L_{RD}}, \quad \text{Eq. 15}$$

where D_{gas} and D_{liq} are the diffusion coefficients of O_3 in the gas- and aqueous phases, respectively.

Expressions for the uptake coefficients given in Eqs. 2 and 3 are now fully constrained by Eqs. 11 and 12. We highlight that the competitive adsorption isotherm defining $\left[I^-_{(ads)}\right]$ in Eq. 5 is necessary to calculate $\left[O_{3(ads)}\right]$ in Eq. 11 and $\left[O_{3(rd)}\right]$ in Eq. 12. Note that the competitive adsorption description in Eq. 5 itself relies on the depletion equation for $[TX_{(bulk)}]$ in Eq. 9.

V. Discussion

By implementing the approach outlined above, a quantitative assessment of the observed kinetics is possible. As shown in Fig. 4, the total uptake calculated by Eq. 4 agrees with the measured uptake coefficients as [TX] increases from 6 μM to 3.2 mM. Individual uptake contributions from the reaction in surface region (Eq. 2) and RD region (Eq. 3) demonstrate that the overall reactivity is dominated by the surface when [TX] < 150 μM, which then becomes increasingly attenuated when [TX] > 150 μM. This attenuation is accompanied by a slight increase in the reactivity of the RD region. This predicted rise in the RD contribution results from the fact that when the surface-reaction dominates, $O_{3(ads)}$ becomes partially depleted at the interface such that the reactivity in the RD region is partially "screened." Importantly, the degree of surface-reaction suppression plateaus when [TX] > 500 μM, indicating the microdroplet surface is saturated by Triton X-100. For this case, the reactivity is dominated by the sub-surface RD region, since I^- is completely displaced from the surface by TX. The $[TX]_0$ where the surface-to-subsurface transition occurs as well as the overall shape of the uptake dependence observed in experiment is reproduced by the analytical expression shown in Eq. 4.

The unique chemical kinetics observed in the experiments arise from two distinct effects related to the nature of the interface and the microscale volume. The first, and most clear, is the increasing displacement of I^- at the air-water interface with increasing [TX]. The potential for I^- displacement by TX has been modeled using a competitive Langmuir adsorption isotherm parametrized from surface-tension measurements of aqueous TX and from molecular dynamics simulations of aqueous I^-.[39] Although a competitive-adsorption framework is utilized, we note that due to the much greater preference for TX to the interface than I^-, TX greatly out-competes I^- for surface area and the surface-reaction uptake dependence on [TX] scales with the TX coverage function. The second microdroplet-related effect is the concentration range over which TX inhibits the surface reaction and the shape of the affected uptake. This range and shape are unique to the depletion of TX within the bulk interior of the microdroplet, which is a

function of the droplet radius and mirrors the surface fractional coverage for microdroplets shown in Fig. 7A.

In comparison to previous works, a similar degree of $I^- + O_3$ reaction suppression was reported by Rouvière et al. in the study of O_3 uptake onto deliquesced submicron KI aerosol with varying amounts of a fatty acid.[65] Fatty acids with larger molecular footprints resulted in larger degrees of reaction suppression, up to over an order of magnitude decrease in overall uptake with increasing surfactant concentration. However, these submicron experiments are not directly comparable to the current work as the fatty acids are included at much higher mass fractions than the current work and exceed their solubility limits. As such, Rouvière et al.[65] observe reaction suppression largely due to surface-film formation rather than monolayer coverage as investigated in the present work. Chemical effects of films and monolayers also become relevant for understanding the reactivity of iodide in the sea-surface microlayer (SSM), which contains a complex mixture of inorganic and surface-active organic molecules. Tinel et al.[66] analyzed the volatile product distributions from O_3 oxidation of simulated seawater and real SSM samples, demonstrating that microlayer composition has a marked effect on I_2 production rates. Similarly, Schneider et al.[67] measured the production of I_2 from the ozone uptake onto aqueous iodide solutions under varying conditions with proxies to seawater and microlayer conditions. While the impact of surfactant adsorption to iodide-chemistry in the SSM is likely significant, we note that the behavior analyzed here applies more directly to concentrated solutions where surface reactions dominate—unlike the dilute $[I^-]$ found in seawater where reactivity is dominated by liquid-diffusion limitations of ozone in the reaction-diffusion region.[68]

We emphasize that the inclusion of Triton X-100 into the previously developed chemical kinetic framework[38] involves no adjustable parameters, and the mechanistic addition of TX relies only on surface-tension measurements[30] analyzed within a Langmuir framework. Although the Langmuir-adsorption description is likely an oversimplification (especially for describing gas-liquid dynamics), the additive behavior of a Langmuir-adsorption description in the current work shows remarkable agreement with experiment. We believe this is the case because TX adsorption to the interface is much more favorable than I^-, while we expect this simplistic model to potentially break down for two (or more) strongly adsorbing reagents, especially in a highly concentrated regime.

VI. Conclusion

Chemical reactivity at interfaces is increasingly invoked to explain broad changes in observed chemical kinetics in environments where surfaces are prominent. Aerosol and microdroplet chemistry, unsurprisingly, is at the forefront of such exploration since these systems often show distinct signatures that indicate the presence of surface reactions and provide a convenient reaction platform for investigating interfacial effects. Here, we present a prototypical example of coupled interfacial phenomena directly inhibiting the $I^- + O_3$ surface reaction in levitated microdroplets. The surfactant Triton X-100 is observed to suppress the surface reaction when the surface coverage fraction is high enough to displace I^- from the air water interface. The TX concentration dependence of O_3 reactive uptake reflects the coverage function of TX—demonstrating a microdroplet-specific signature due to the bulk-depletion effect of TX adsorption to the air-water interface. An analytical expression for reactive uptake on the aqueous surface and within the sub-surface region is derived and based on a previously developed framework. This work demonstrates how insights into molecular timescales of mass transfer across interfaces, combined with macroscopic surface tension measurements, inform on chemical reactivity in micron-scale compartments containing a mixture of organic and inorganic components.

Supporting Information: Overview of experimental setup, a description of the model framework and kinetic simulations, and further details on the steady-state approach used to derive the analytical uptake expressions.

Acknowledgements: This work was supported by the Condensed Phase and Interfacial Molecular Science Program (CPIMS), in the Chemical Sciences Geosciences and Biosciences Division of the Office of Basic Energy Sciences of the U.S. Department of Energy under Contract No. DE-AC02-05CH11231.

References

(1) Wei, Z.; Li, Y.; Cooks, R. G.; Yan, X. Accelerated Reaction Kinetics in Microdroplets: Overview and Recent Developments. *Annual Review of Physical Chemistry* **2020**, *71* (Volume 71, 2020), 31–51. https://doi.org/10.1146/annurev-physchem-121319-110654.

(2) Brown, E. K.; Rovelli, G.; Wilson, K. R. pH Jump Kinetics in Colliding Microdroplets: Accelerated Synthesis of Azamonardine from Dopamine and Resorcinol. *Chemical Science* **2023**, *14* (23), 6430–6442. https://doi.org/10.1039/D3SC01576A.

(3) Wilson, K. R.; Prophet, A. M.; Rovelli, G.; Willis, M. D.; Rapf, R. J.; Jacobs, M. I. A Kinetic Description of How Interfaces Accelerate Reactions in Micro-Compartments. *Chemical Science* **2020**, *11* (32), 8533–8545. https://doi.org/10.1039/D0SC03189E.

(4) Nam, I.; Lee, J. K.; Nam, H. G.; Zare, R. N. Abiotic Production of Sugar Phosphates and Uridine Ribonucleoside in Aqueous Microdroplets. *Proceedings of the National Academy of Sciences* **2017**, *114* (47), 12396–12400. https://doi.org/10.1073/pnas.1714896114.

(5) Jacobs, M. I.; Davis, R. D.; Rapf, R. J.; Wilson, K. R. Studying Chemistry in Micro-Compartments by Separating Droplet Generation from Ionization. *Journal of the American Society for Mass Spectrometry* **2019**, *30* (2), 339–343. https://doi.org/10.1007/s13361-018-2091-y.
(6) Gallo, A.; Farinha, A. S. F.; Dinis, M.; Emwas, A.-H.; Santana, A.; Nielsen, R. J.; Goddard, W. A.; Mishra, H. The Chemical Reactions in Electrosprays of Water Do Not Always Correspond to Those at the Pristine Air–Water Interface. *Chemical Science* **2019**, *10* (9), 2566–2577. https://doi.org/10.1039/C8SC05538F.
(7) Rovelli, G.; Jacobs, M. I.; Willis, M. D.; Rapf, R. J.; Prophet, A. M.; Wilson, K. R. A Critical Analysis of Electrospray Techniques for the Determination of Accelerated Rates and Mechanisms of Chemical Reactions in Droplets. *Chemical Science* **2020**, *11* (48), 13026–13043. https://doi.org/10.1039/D0SC04611F.
(8) J. Chen, C.; R. Williams, E. The Role of Analyte Concentration in Accelerated Reaction Rates in Evaporating Droplets. *Chemical Science* **2023**, *14* (18), 4704–4713. https://doi.org/10.1039/D3SC00259D.
(9) Lee, J. K.; Walker, K. L.; Han, H. S.; Kang, J.; Prinz, F. B.; Waymouth, R. M.; Nam, H. G.; Zare, R. N. Spontaneous Generation of Hydrogen Peroxide from Aqueous Microdroplets. *Proceedings of the National Academy of Sciences* **2019**, *116* (39), 19294–19298. https://doi.org/10.1073/pnas.1911883116.
(10) Xiong, H.; Lee, J. K.; Zare, R. N.; Min, W. Strong Electric Field Observed at the Interface of Aqueous Microdroplets. *J. Phys. Chem. Lett.* **2020**, *11* (17), 7423–7428. https://doi.org/10.1021/acs.jpclett.0c02061.
(11) Martins-Costa, M. T. C.; Ruiz-López, M. F. Probing Solvation Electrostatics at the Air–Water Interface. *Theor Chem Acc* **2023**, *142* (3), 29. https://doi.org/10.1007/s00214-023-02969-y.
(12) Ahmad Eatoo, M.; Mishra, H. Busting the Myth of Spontaneous Formation of H 2 O 2 at the Air–Water Interface: Contributions of the Liquid–Solid Interface and Dissolved Oxygen Exposed. *Chemical Science* **2024**, *15* (9), 3093–3103. https://doi.org/10.1039/D3SC06534K.
(13) Heindel, J. P.; LaCour, R. A.; Head-Gordon, T. The Role of Charge in Microdroplet Redox Chemistry. *Nat Commun* **2024**, *15* (1), 3670. https://doi.org/10.1038/s41467-024-47879-0.
(14) Chen, C. J.; Williams, E. Are Hydroxyl Radicals Spontaneously Generated in Unactivated Water Droplets? *Angewandte Chemie International Edition n/a* (n/a), e202407433. https://doi.org/10.1002/anie.202407433.
(15) Valsaraj, K. T. Hydrophobic Compounds in the Environment: Adsorption Equilibrium at the Air-Water Interface. *Water Research* **1994**, *28* (4), 819–830. https://doi.org/10.1016/0043-1354(94)90088-4.
(16) Vaikuntanathan, S.; Shaffer, P. R.; Geissler, P. L. Adsorption of Solutes at Liquid–Vapor Interfaces: Insights from Lattice Gas Models. *Faraday Discuss.* **2013**, *160* (0), 63–74. https://doi.org/10.1039/C2FD20106B.
(17) Otten, D. E.; Shaffer, P. R.; Geissler, P. L.; Saykally, R. J. Elucidating the Mechanism of Selective Ion Adsorption to the Liquid Water Surface. *Proceedings of the National Academy of Sciences* **2012**, *109* (3), 701–705. https://doi.org/10.1073/pnas.1116169109.
(18) Goss, K.-U. Predicting Adsorption of Organic Chemicals at the Air−Water Interface. *J. Phys. Chem. A* **2009**, *113* (44), 12256–12259. https://doi.org/10.1021/jp907347p.
(19) Devlin, S. W.; Benjamin, I.; Saykally, R. J. On the Mechanisms of Ion Adsorption to Aqueous Interfaces: Air-Water vs. Oil-Water. *Proceedings of the National Academy of Sciences* **2022**, *119* (42), e2210857119. https://doi.org/10.1073/pnas.2210857119.

(20) Zou, Y.-S.; Fukuta, N. The Effect of Diffusion Kinetics on the Supersaturation in Clouds. *Atmospheric Research* **1999**, *52* (1), 115–141. https://doi.org/10.1016/S0169-8095(99)00025-3.
(21) Bell, A. K.; Kind, J.; Hartmann, M.; Kresse, B.; Höfler, M. V.; Straub, B. B.; Auernhammer, G. K.; Vogel, M.; Thiele, C. M.; Stark, R. W. Concentration Gradients in Evaporating Binary Droplets Probed by Spatially Resolved Raman and NMR Spectroscopy. *Proceedings of the National Academy of Sciences* **2022**, *119* (15), e2111989119. https://doi.org/10.1073/pnas.2111989119.
(22) Karmakar, T.; Finney, A. R.; Salvalaglio, M.; Yazaydin, A. O.; Perego, C. Non-Equilibrium Modeling of Concentration-Driven Processes with Constant Chemical Potential Molecular Dynamics Simulations. *Acc. Chem. Res.* **2023**, *56* (10), 1156–1167. https://doi.org/10.1021/acs.accounts.2c00811.
(23) Prisle, N. L.; Raatikainen, T.; Laaksonen, A.; Bilde, M. Surfactants in Cloud Droplet Activation: Mixed Organic-Inorganic Particles. *Atmospheric Chemistry and Physics* **2010**, *10* (12), 5663–5683. https://doi.org/10.5194/acp-10-5663-2010.
(24) Ruehl, C. R.; Davies, J. F.; Wilson, K. R. An Interfacial Mechanism for Cloud Droplet Formation on Organic Aerosols. *Science* **2016**, *351* (6280), 1447–1450. https://doi.org/10.1126/science.aad4889.
(25) Ovadnevaite, J.; Zuend, A.; Laaksonen, A.; Sanchez, K. J.; Roberts, G.; Ceburnis, D.; Decesari, S.; Rinaldi, M.; Hodas, N.; Facchini, M. C.; Seinfeld, J. H.; O' Dowd, C. Surface Tension Prevails over Solute Effect in Organic-Influenced Cloud Droplet Activation. *Nature* **2017**, *546* (7660), 637–641. https://doi.org/10.1038/nature22806.
(26) Davies, J. F.; Zuend, A.; Wilson, K. R. Technical Note: The Role of Evolving Surface Tension in the Formation of Cloud Droplets. *Atmospheric Chemistry and Physics* **2019**, *19* (5), 2933–2946. https://doi.org/10.5194/acp-19-2933-2019.
(27) Lin, J. J.; Kristensen, T. B.; Calderón, S. M.; Malila, J.; Prisle, N. L. Effects of Surface Tension Time-Evolution for CCN Activation of a Complex Organic Surfactant. *Environ. Sci.: Processes Impacts* **2020**, *22* (2), 271–284. https://doi.org/10.1039/C9EM00426B.
(28) McGraw, R.; Wang, J. Surfactants and Cloud Droplet Activation: A Systematic Extension of Köhler Theory Based on Analysis of Droplet Stability. *The Journal of Chemical Physics* **2021**, *154* (2), 024707. https://doi.org/10.1063/5.0031436.
(29) Prisle, N. L. Surfaces of Atmospheric Droplet Models Probed with Synchrotron XPS on a Liquid Microjet. *Acc. Chem. Res.* **2024**, *57* (2), 177–187. https://doi.org/10.1021/acs.accounts.3c00201.
(30) Bzdek, B. R.; Reid, J. P.; Malila, J.; Prisle, N. L. The Surface Tension of Surfactant-Containing, Finite Volume Droplets. *Proceedings of the National Academy of Sciences* **2020**, *117* (15), 8335–8343. https://doi.org/10.1073/pnas.1915660117.
(31) Bain, A.; Ghosh, K.; Prisle, N. L.; Bzdek, B. R. Surface-Area-to-Volume Ratio Determines Surface Tensions in Microscopic, Surfactant-Containing Droplets. *ACS Cent. Sci.* **2023**, *9* (11), 2076–2083. https://doi.org/10.1021/acscentsci.3c00998.
(32) Singh, M.; Jones, S. H.; Kiselev, A.; Duft, D.; Leisner, T. The Viscosity and Surface Tension of Supercooled Levitated Droplets Determined by Excitation of Shape Oscillations. *Atmospheric Measurement Techniques* **2023**, *16* (21), 5205–5215. https://doi.org/10.5194/amt-16-5205-2023.
(33) Bain, A.; Lalemi, L.; Croll Dawes, N.; Miles, R. E. H.; Prophet, A. M.; Wilson, K. R.; Bzdek, B. R. Surfactant Partitioning Dynamics in Freshly Generated Aerosol Droplets. *J. Am. Chem. Soc.* **2024**. https://doi.org/10.1021/jacs.4c03041.
(34) Gao, X.-F.; Nathanson, G. M. Exploring Gas–Liquid Reactions with Microjets: Lessons We Are Learning. *Acc. Chem. Res.* **2022**, *55* (23), 3294–3302. https://doi.org/10.1021/acs.accounts.2c00602.

(35) Galib, M.; Limmer, D. T. Reactive Uptake of N2O5 by Atmospheric Aerosol Is Dominated by Interfacial Processes. *Science* **2021**, *371* (6532), 921–925. https://doi.org/10.1126/science.abd7716.
(36) Qiu, L.; Wei, Z.; Nie, H.; Cooks, R. G. Reaction Acceleration Promoted by Partial Solvation at the Gas/Solution Interface. *ChemPlusChem* **2021**, *86* (10), 1362–1365. https://doi.org/10.1002/cplu.202100373.
(37) Martins-Costa, M. T. C.; Ruiz-López, M. F. Electrostatics and Chemical Reactivity at the Air–Water Interface. *J. Am. Chem. Soc.* **2023**, *145* (2), 1400–1406. https://doi.org/10.1021/jacs.2c12089.
(38) Prophet, A. M.; Polley, K.; Van Berkel, G. J.; Limmer, D. T.; Wilson, K. R. Iodide Oxidation by Ozone at the Surface of Aqueous Microdroplets. *Chemical Science* **2024**, *15* (2), 736–756. https://doi.org/10.1039/D3SC04254E.
(39) Prophet, A. M.; Polley, K.; Brown, E. K.; Limmer, D. T.; Wilson, K. R. Distinguishing Surface and Bulk Reactivity: Concentration-Dependent Kinetics of Iodide Oxidation by Ozone in Microdroplets. *J. Phys. Chem. A* **2024**, *128* (41), 8970–8982. https://doi.org/10.1021/acs.jpca.4c05129.
(40) Bhujel, M.; L. Marshall, D.; T. Maccarone, A.; I. McKinnon, B.; J. Trevitt, A.; Silva, G. da; J. Blanksby, S.; J. Poad, B. L. Gas Phase Reactions of Iodide and Bromide Anions with Ozone: Evidence for Stepwise and Reversible Reactions. *Physical Chemistry Chemical Physics* **2020**, *22* (18), 9982–9989. https://doi.org/10.1039/D0CP01498B.
(41) Limmer, D. T.; Götz, A. W.; Bertram, T. H.; Nathanson, G. M. Molecular Insights into Chemical Reactions at Aqueous Aerosol Interfaces. *Annual Review of Physical Chemistry* **2024**, *75* (Volume 75, 2024), 111–135. https://doi.org/10.1146/annurev-physchem-083122-121620.
(42) Hoigné, J.; Bader, H.; Haag, W. R.; Staehelin, J. Rate Constants of Reactions of Ozone with Organic and Inorganic Compounds in Water—III. Inorganic Compounds and Radicals. *Water Research* **1985**, *19* (8), 993–1004. https://doi.org/10.1016/0043-1354(85)90368-9.
(43) Liu, Q.; Schurter, L. M.; Muller, C. E.; Aloisio, S.; Francisco, J. S.; Margerum, D. W. Kinetics and Mechanisms of Aqueous Ozone Reactions with Bromide, Sulfite, Hydrogen Sulfite, Iodide, and Nitrite Ions. *Inorg. Chem.* **2001**, *40* (17), 4436–4442. https://doi.org/10.1021/ic000919j.
(44) Brown, L. V.; Pound, R. J.; Ives, L. S.; Jones, M. R.; Andrews, S. J.; Carpenter, L. J. Negligible Temperature Dependence of the Ozone–Iodide Reaction and Implications for Oceanic Emissions of Iodine. *Atmospheric Chemistry and Physics* **2024**, *24* (7), 3905–3923. https://doi.org/10.5194/acp-24-3905-2024.
(45) Makievski, A. V.; Fainerman, V. B.; Joos, P. Dynamic Surface Tension of Micellar Triton X-100 Solutions by the Maximum-Bubble-Pressure Method. *Journal of Colloid and Interface Science* **1994**, *166* (1), 6–13. https://doi.org/10.1006/jcis.1994.1264.
(46) Fainerman, V. B.; Lylyk, S. V.; Aksenenko, E. V.; Makievski, A. V.; Petkov, J. T.; Yorke, J.; Miller, R. Adsorption Layer Characteristics of Triton Surfactants: 1. Surface Tension and Adsorption Isotherms. *Colloids and Surfaces A: Physicochemical and Engineering Aspects* **2009**, *334* (1), 1–7. https://doi.org/10.1016/j.colsurfa.2008.09.015.
(47) Robinson, J. E.; Sutton, C. M.; Reid, G. F. Dilute Triton X-100 in Water as a Reference Liquid for Hydrometer Calibration Using Cuckow's Method. *Measurement* **2014**, *57*, 132–137. https://doi.org/10.1016/j.measurement.2014.08.001.
(48) Willis, M. D.; Rovelli, G.; Wilson, K. R. Combining Mass Spectrometry of Picoliter Samples with a Multicompartment Electrodynamic Trap for Probing the Chemistry of Droplet Arrays. *Anal. Chem.* **2020**, *92* (17), 11943–11952. https://doi.org/10.1021/acs.analchem.0c02343.

(49) Willis, M. D.; Wilson, K. R. Coupled Interfacial and Bulk Kinetics Govern the Timescales of Multiphase Ozonolysis Reactions. *J. Phys. Chem. A* **2022**, *126* (30), 4991–5010. https://doi.org/10.1021/acs.jpca.2c03059.
(50) Kaur Kohli, R.; Van Berkel, G. J.; Davies, J. F. An Open Port Sampling Interface for the Chemical Characterization of Levitated Microparticles. *Anal. Chem.* **2022**, *94* (8), 3441–3445. https://doi.org/10.1021/acs.analchem.1c05550.
(51) Jacobs, M. I.; Davies, J. F.; Lee, L.; Davis, R. D.; Houle, F.; Wilson, K. R. Exploring Chemistry in Microcompartments Using Guided Droplet Collisions in a Branched Quadrupole Trap Coupled to a Single Droplet, Paper Spray Mass Spectrometer. *Analytical Chemistry* **2017**, *89* (22), 12511–12519. https://doi.org/10.1021/acs.analchem.7b03704.
(52) Davies, J. F. Mass, Charge, and Radius of Droplets in a Linear Quadrupole Electrodynamic Balance. *Aerosol Science and Technology* **2019**, *53* (3), 309–320. https://doi.org/10.1080/02786826.2018.1559921.
(53) Smith, J. D.; Kroll, J. H.; Cappa, C. D.; Che, D. L.; Liu, C. L.; Ahmed, M.; Leone, S. R.; Worsnop, D. R.; Wilson, K. R. The Heterogeneous Reaction of Hydroxyl Radicals with Sub-Micron Squalane Particles: A Model System for Understanding the Oxidative Aging of Ambient Aerosols. *Atmospheric Chemistry and Physics* **2009**, *9* (9), 3209–3222. https://doi.org/10.5194/acp-9-3209-2009.
(54) Kuramoto, Y. Effects of Diffusion on the Fluctuations in Open Chemical Systems. *Progress of Theoretical Physics* **1974**, *52* (2), 711–713. https://doi.org/10.1143/PTP.52.711.
(55) Houle, F. A.; Wiegel, A. A.; Wilson, K. R. Predicting Aerosol Reactivity Across Scales: From the Laboratory to the Atmosphere. *Environ. Sci. Technol.* **2018**, *52* (23), 13774–13781. https://doi.org/10.1021/acs.est.8b04688.
(56) Wilson, K. R.; Prophet, A. M. Chemical Kinetics in Microdroplets. *Annual Review of Physical Chemistry* **2024**, *75*, 185–208. https://doi.org/10./1146/annurev-physchem-052623-120718.
(57) Wilson, K. R.; Prophet, A. M.; Willis, M. D. A Kinetic Model for Predicting Trace Gas Uptake and Reaction. *J. Phys. Chem. A* **2022**, *126* (40), 7291–7308. https://doi.org/10.1021/acs.jpca.2c03559.
(58) Masel, R. I. *Principles of Adsorption and Reaction on Solid Surfaces*; John Wiley & Sons, 1996.
(59) Szyszkowski, B. von. Experimentelle Studien über kapillare Eigenschaften der wässerigen Lösungen von Fettsäuren. *Zeitschrift für Physikalische Chemie* **1908**, *64U* (1), 385–414. https://doi.org/10.1515/zpch-1908-6425.
(60) He, Y.; Yazhgur, P.; Salonen, A.; Langevin, D. Adsorption–Desorption Kinetics of Surfactants at Liquid Surfaces. *Advances in Colloid and Interface Science* **2015**, *222*, 377–384. https://doi.org/10.1016/j.cis.2014.09.002.
(61) Alvarez, N. J.; Walker, L. M.; Anna, S. L. Diffusion-Limited Adsorption to a Spherical Geometry: The Impact of Curvature and Competitive Time Scales. *Phys. Rev. E* **2010**, *82* (1), 011604. https://doi.org/10.1103/PhysRevE.82.011604.
(62) Polley, K.; Wilson, K. R.; Limmer, D. T. On the Statistical Mechanics of Mass Accommodation at Liquid–Vapor Interfaces. *J. Phys. Chem. B* **2024**, *128* (17), 4148–4157. https://doi.org/10.1021/acs.jpcb.4c00899.
(63) Fuchs, N. A.; Sutugin, A. G. High-Dispersed Aerosols. In *Topics in Current Aerosol Research*; Hidy, G. M., Brock, J. R., Eds.; International Reviews in Aerosol Physics and Chemistry; Pergamon, 1971; p 1. https://doi.org/10.1016/B978-0-08-016674-2.50006-6.
(64) Fick, A. V. On Liquid Diffusion. *The London, Edinburgh, and Dublin Philosophical Magazine and Journal of Science* **1855**, *10* (63), 30–39. https://doi.org/10.1080/14786445508641925.

(65) Rouvière, A.; Ammann, M. The Effect of Fatty Acid Surfactants on the Uptake of Ozone to Aqueous Halogenide Particles. *Atmospheric Chemistry and Physics* **2010**, *10* (23), 11489–11500. https://doi.org/10.5194/acp-10-11489-2010.
(66) Tinel, L.; Adams, T. J.; Hollis, L. D. J.; Bridger, A. J. M.; Chance, R. J.; Ward, M. W.; Ball, S. M.; Carpenter, L. J. Influence of the Sea Surface Microlayer on Oceanic Iodine Emissions. *Environ. Sci. Technol.* **2020**, *54* (20), 13228–13237. https://doi.org/10.1021/acs.est.0c02736.
(67) Schneider, S. R.; Lakey, P. S. J.; Shiraiwa, M.; Abbatt, J. P. D. Iodine Emission from the Reactive Uptake of Ozone to Simulated Seawater. *Environ. Sci.: Processes Impacts* **2023**, *25* (2), 254–263. https://doi.org/10.1039/D2EM00111J.
(68) Schneider, S. R.; Lakey, P. S. J.; Shiraiwa, M.; Abbatt, J. P. D. Reactive Uptake of Ozone to Simulated Seawater: Evidence for Iodide Depletion. *The Journal of Physical Chemistry A* **2020**, *124* (47), 9844–9853. https://doi.org/10.1021/ACS.JPCA.0C08917.